CHEMISTRY & SUSTAINABILITY

CHEMSUSCHEM

ENERGY & MATERIALS

Accepted Article

Title: A robust molecular catalyst generated in-situ for photo- and electrochemical water oxidation

Authors: Hussein A. Younus, Nazir Ahmad, Adeel H. Chughtai, Matthias Vandichel, Michael Busch, Kristof Van Hecke, Mekhman Yusubov, Shaoxian Song, and Francis Verpoort

To be cited as: *ChemSusChem* 10.1002/cssc.201601477

Link to VoR: http://dx.doi.org/10.1002/cssc.201601477

A Journal of

ChemPubSoc Europe

WILEY-VCH

www.chemsuschem.org

A robust molecular catalyst generated in-situ for photo- and electrochemical water oxidation

Hussein. A. Younus,[a,b,c]† Nazir Ahmad,[a,b,c]† Adeel H. Chughtai,[a] Matthias Vandichel,[e, f] Michael Busch,[f] Kristof Van Hecke,[d] Mekhman Yusubov,[c] Shaoxian Song,[b] Francis Verpoort.*[a,b,c,d]

Abstract: Water splitting is the key step towards artificial photosystems for solar energy conversion and storage in the form of chemical bonding. The oxidation of water is the bottle-neck of this process that hampers its practical utility and hence efficient, robust, and also easy to make catalytic systems based on cheap and earth abundant materials are of exceptional importance. Here, we present an *in-situ* generated cobalt catalyst [Co(II)$(TCA)_2(H_2O)_2$] (where TCA = 1-Mesityl-1,2,3-1H-triazole-4-carboxylate) that efficiently conducts photochemical water oxidation at near-neutral conditions. The catalyst showed high stability under photolytic conditions for more than 3 h of photoirradiation. During electrochemical water oxidation, the catalytic system assembled a catalyst film, which proved not to be cobalt oxide/hydroxide as normally expected, but instead and for the first time, generated a molecular cobalt complex incorporating the organic ligand bound to cobalt ions. The catalyst film exhibited low overpotential for electrocatalytic water oxidation (360 mV) and high oxygen evolution peak current density of 9 mA cm^{-2} and 2.7 mA cm^{-2} on GC and ITO electrodes at only 1.49 and 1.39 V (*vs*. NHE), respectively, under neutral conditions. Our finding, exemplified on the *in-situ* generated cobalt complex, might be applicable to other molecular systems and suggests that the formation of catalytic film in electrochemical water oxidation experiments is not always indication of the catalyst decomposition and formation of nanoparticles.

[a] Dr. H. A. Younus, Dr. N. Ahmad, Dr. A. H. Chughtai, Prof. F. Verpoort
State Key Laboratory of Advanced Technology for Materials Synthesis and Processing
Wuhan University of Technology
Wuhan-430070, China
E-mail: francis.verpoort@ghent.ac.k
[b] Dr. H. A. Younus, Dr. N. Ahmad, Prof. S. Song, Prof. F. Verpoort
School of Resources and Environmental Engineering
Wuhan University of Technology
Wuhan-430070, China
[c] Dr. H. A. Younus, Dr. N. Ahmad, Prof. F. Verpoort
National Research Tomsk Polytechnic University
Lenin Avenue 30, Tomsk-634050, Russia
[d] Prof. K. Van Hecke, Prof. F. Verpoort
Department of Inorganic and Physical Chemistry, Laboratory of Organometallic Chemistry and Catalysis
Ghent University
Krijgslaan 281 (S-3), 9000 Ghent, Belgium
[e] Prof. M. Vandichel
Center for Molecular Modeling
Ghent University
Technology Park 903, 9052 Zwijnaarde, Belgium
[f] Dr. M. Vandichel, Dr. M. Busch
Department of Physics and Competence Center for Catalysis
Chalmers University of Technology
Fysikgränd 3, S- Göteborg
[†] These authors contributed equally to this work.
Supporting information for this article is given via a link at the end of the document.

Introduction

Nature, represented in plants and few microorganisms, have given an extraordinary way to utilize the solar energy for making life on our globe and gave us an ideal blueprint to mimic their comportment. Inspired by the natural oxygen-evolving complex (OEC) in photosystem II,[1] remarkable efforts have been devoted towards the development of single-site as well as multinuclear transition metal complexes enabling water oxidation for artificial photosynthesis.[2] Several molecular catalytic systems for water oxidation have been developed, that are based on Ru,[3] Ir,[4] Co,[5] Cu,[6] Mn,[7] Fe,[8] and Ni[9]. Moreover, tremendous efforts have been devoted to materials based on transition metal oxides and hydroxides.[10] Because of cost considerations, the development of highly active catalysts for water oxidation that are based on earth-abundant transition metals is essential for practical applications and would greatly enhance the commercial viability of solar energy.[8b, 11] Although cobalt is significantly less abundant (20– 30 ppm) than Fe (6.3%), Mn (0.1%), Ni (90 ppm), or Cu (68 ppm) in the outer layer of the earth crust, it is now the most researched metal for its catalytic power for both water oxidation and hydrogen evolution.[12] Catalyst robustness, effectiveness, and benign operating conditions (such as neutral pH, low to moderate overpotential, temperature, *etc*.) make cobalt based-catalysts the most promising candidates for both water oxidation and reduction.[12a]

Molecular catalytic systems are well recognized for their tunable redox properties and facile characterizations of their active intermediates, which are necessary to the related mechanistic studies. However, the identity of the active catalyst must be investigated in depth before a detailed interrogation of the WOC mechanism. The identification of the real catalyst is extremely challenging especially for the studies on cobalt-based homogeneous WOCs.[5b, 13] This is mainly due to the fact that small amounts of cobalt oxide may be produced from the decomposition of the molecular catalyst which work as an efficient catalyst during the water oxidation reaction.[13b, 14] Indeed, some catalysts that were thought to be real WOCs have subsequently been demonstrated to act as precursors of heterogeneous materials, which are the active catalysts.[13b, 15] In other cases, the cubane Co_4O_4 clusters in $Co_4O_4(Ac)_4(py)_4$ were primarily introduced as homogeneous WOCs, but recently it has been confirmed that the observed water oxidation activity originates from Co(II) impurities rather than the Co_4O_4 clusters.[16] Nonetheless, there are also examples of cobalt complexes that do function as homogeneous, molecular water oxidation catalysts (WOCs).[11b, 17]

All cobalt WOCs reported so far, in both of the homogenous and heterogeneous systems, are mainly based on polydentate ligands which are likely to be necessary for stabilizing Co ions in higher oxidation states. In most cases, the ligand is rigid which might prevent the complex from any expected conformations

during the catalytic mechanism to finally deliver oxygen. Additionally, most of the reported homogenous molecular cobalt complexes, if not all, are based on tetra- or pentadentate ligands that require a special design and may be not easy to tune or even to synthesize. This inspired us to explore cobalt complexes based on a bidentate ligand to see whether the polydentate ligand nature is crucial to maintain the homogeneity of the catalytic system or not. Moreover, the strong influence of an anionic carboxylate ligand on ruthenium WOCs, proved to be very effective to stabilize higher oxidation states, resulting in unprecedentedly high reaction rates with a turnover frequency comparable with the rate of the oxygen-evolving complex of natural photosystem.[18]

Herein we present the *in-situ* generated mononuclear cobalt(II) complex $[Co(TCA)_2(H_2O)_2]$ (1; TCA= 1-mesityl-triazole-4-carboxylate) as a molecular catalyst for both electrochemical and photochemical water oxidation. The catalyst was prepared *in-situ* from commercially available cobalt acetate and 1-aryl-1H-1,2,3-triazole-4-carboxylic acid in an acetate buffer solution at near neutral conditions (pH 6-7). Several lines of evidence demonstrate that the system works as molecular catalyst under visible light irradiation, with $Ru(bpy)_3^{2+}$ as photosensitizer and persulfate as sacrificial electron acceptor such as DLS, ESI-MS, ^{1}H-NMR, and FT-IR. Moreover, the catalytic system generates a catalytic active film on the GC electrode that is highly efficient for electrocatalytic water oxidation. The current densities reach ~9 mA/cm^2 at only 1.49 V (vs. NHE) at pH 6 (~600 mV overpotential). Several characterization techniques including SEM, EDX, XPS, and Raman spectroscopy of the deposited film on both glassy carbon (GC) and indium doped tin oxide (ITO) electrodes revealed that the brown film deposition is not indicative for CoOx nanoparticle formation during the electrochemical water oxidation as normally expected but it might be due to the formation of a molecular specie incorporating the organic ligand bound to the cobalt ions. More interestingly, the deposited brown film could be dissolved in organic solvents such methanol and chloroform that enabled its further characterizations *via* ^{1}H-NMR and FT-IR, that match completely with the isolated product after photochemical water oxidation experiments.

Results and Discussion

Synthesis and characterizations

Ligand design and consequently catalyst optimization are influential for O_2 production and many multi-coordinating ligands are accessible to produce new catalytic systems. To develop a low-cost and viable catalyst for water oxidation reaction, we paid attention to use the earth-abundant metal cobalt complexes that can be prepared in the aqueous medium on direct mixing from easily accessible sources. The straightforward construction of a triazole ring along with possible immobilization on any azide or alkyne functionalized surface also is very attractive for using a substituted triazole ring as a bidentate ligand for WO.[19] The bidentate ligand, 1-aryl-1H-1,2,3-triazole-4-carboxylic acid, was readily prepared *via* copper catalyzed azide-alkyne cycloaddition "click reaction" of aryl azide and propiolic acid. Then, the catalyst was prepared by adding cobalt acetate to a pre-dissolved ligand in acetate buffer. The *in-situ* catalyst formation was established based on UV-Vis spectroscopy, ESI-MS, and also confirmed in the solid state from X-ray single crystal analysis.

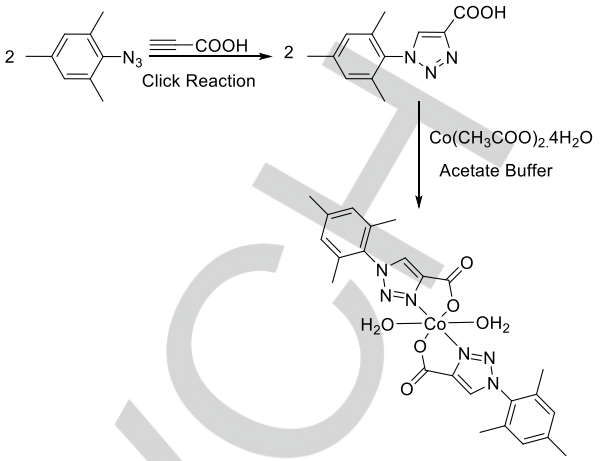

Scheme 1. Synthesis of $[Co(TCA)_2.2H_2O]$ (**1**).

In the UV-Vis absorption spectra of TCA ligand, there are two weak absorption bands with maxima at 269 and 274 nm, in both MeOH and acetate buffer (pH 6) (Figure S1), while cobalt acetate showed an absorption peak at 519 nm. Mixing ligand and cobalt acetate in a 2:1 ratio in buffer solution, directly resulted in complete disappearance of the peak corresponding to cobalt acetate and the appearance of a new broad peak from 580 - 400 nm with a maximum at 483 nm (Figure S2). The new peak did not differ in time after several scans at different intervals and was in excellent agreement with the peak of the as-synthesized complex. Using different ratios of ligand to cobalt ions leads to no difference in the UV-Vis spectra of the complexes (Figure S3). The color of the different *in-situ* generated complexes in acetate buffer are identical except in case of 1:1 ratio, the color remains light pink deriving from the cobalt acetate source. This can be interpreted as the result of two ligands coordinating to one cobalt ion and the coexistence of free cobalt ions. This point was also confirmed by isolating the same product with different ligand to metal ratios as was indicated by solid state X-ray single crystal analysis. UV-Vis spectroscopy did not show a clear difference in case of 1:1 ratio due to the low molar absorptivity of cobalt acetate. Trials to follow the complex formation under the same conditions (in acetate buffer prepared in D_2O) failed due to the instant precipitation of the complex at the higher concentrations used for NMR sampling.

Slow evaporation of an aqueous complex solution (5 mM), from acetate buffer, results in light brown crystals within two days. The ESI-MS of the separated catalyst crystals exposed a strong peak at *m/z* = 553.42 corresponding to $[Co(TCA)_2(H_2O)_2]$ (M^+-$2H^+$). Interestingly, crystals suitable for X-ray crystallography were obtained from low concentrated solutions (1mM) within 3-4 weeks from acetate buffer (pH 6), supporting the notion that the complex structure is highly robust in buffer solution for long time. Compound **1** crystallized in the centro-symmetric triclinic space group *P*-1. As obvious from this space group, the inverted structure or mirror image is present in the crystal for 50%. But the asymmetric unit contains two halves of crystallographically independent, but isostructural $Co(TCA)_2(H_2O)_2$ complexes, with both the Co(II) ions located on inversion centers, together with two solvent water molecules. Hence a complete $Co(TCA)_2(H_2O)_2$ complex is built up by an inversion center itself. As a consequence, this means that the inverted structures of the first $Co(TCA)_2(H_2O)_2$ complex, as well as of the second complex, are exactly the same and can be perfectly superposed with each

other, preserving the configuration (see Figure S5). So it is not likely that induced chirality might influence the efficiency of catalysis. Each cobalt center exhibits an octahedral coordination geometry, *i.e.* two TCA ligands are bidentately coordinating through both nitrogen and carboxylate-oxygen donor atoms, forming the octahedron equatorial plane, along with two aqua ligands, occupying the axial positions (Figure 1). The Co-O and Co-N distances range from 2.070(3)-2.124(3) Å and 2.115(3)-2.138(3) Å, respectively. In the packing, π-π stacking interactions are observed between the aromatic triazole and mesityl rings (centroid-centroid distances in the range of 5.053(2) - 5.948(2) Å. CH-π interactions are observed between mesityl rings (C-centroid distances between 3.798(5) and 3.893(5) Å). The two cobalt centers prominently feature the presence of an exchangeable two aqua-coordination site on each of Co(II) ions. Most likely, the use of the flexible bidentate coordinating ligands allow the ligand to keep constantly coordinated to the metal center within the complete catalytic cycle. Another feature of the catalyst structure is the sheet-like hydrogen bond network in the (010) plane, which interlocks the oxo bridges, coordinated water and solvent water molecules (Figure S6).

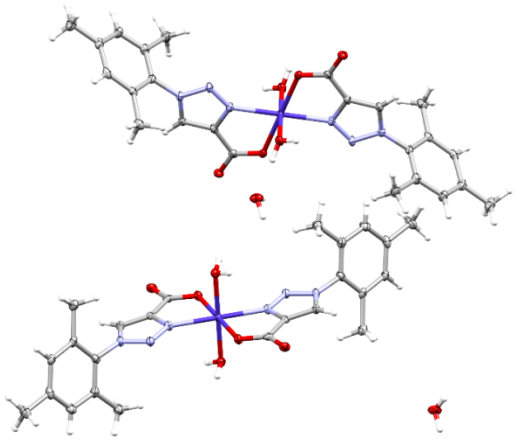

Figure 1. Thermal ellipsoid plot of 1 (with 50 % probability level).

Electrocatalytic Investigations

We started our study by investigating the electrochemical properties of cobalt acetate in acetate buffer (pH 6.0-6.03). A 1mM solution of cobalt acetate showed an irreversible current wave with an onset potential of ~1.15 V *vs.* Ag/AgCl (All potentials presented in this article are referenced to Ag/AgCl electrode). The current reaches ~ 125 μA at 1.3 V in the first scan, with no substantial increase in the catalytic current with subsequent 100 CV scans in the range 0-1.3 V (Figure 2A). Linear sweep voltammetry (LSV) with a fresh glassy carbon electrode (GCE) exhibited relatively high catalytic current ~192 μA at 1.3 V and the catalytic oxidation wave did not show significant change after 100 scans (Figure 2B). The scanning electron microscopy (SEM) topography of the electrodeposited materials on the GCE surface showed the formation of an amorphous powder similar to material reported recently in case of using Indium-doped Tin oxide (ITO) electrode that was proved to be cobalt oxide (Figure S7).[20] Nevertheless, based on LSV data, monitored after the use of GCE for several CV scans, the growth of these materials is very slow. The energy dispersive X-ray spectroscopy (EDX) analysis enabled the determination of the elemental composition of the deposited material (Figure S7). The data confirm the presence of cobalt, sodium, and oxygen. The oxygen to cobalt ratio in the deposited material is consistent with the formation of an oxide/hydroxide film. Moreover, when the GCE was removed from the catalyst solution after 100 CV scans and thoroughly rinsed with water then placed into cobalt-free acetate buffer solution displayed nearly the same catalytic current as observed when the electrode was used in presence of cobalt acetate. This behavior supports the hypothesis of cobalt oxide/hydroxide film formation on the surface of GCE.

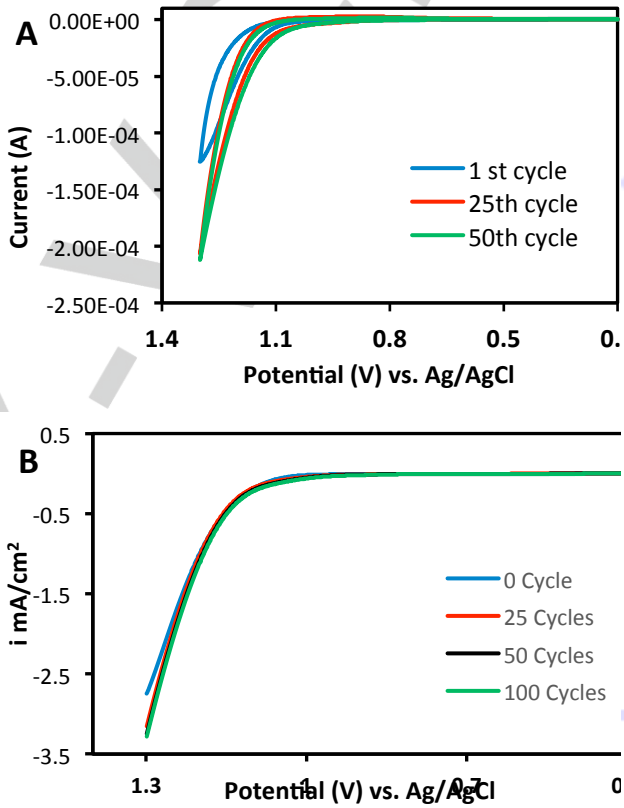

Figure 2. A). Cyclic voltammogram of 1 mM cobalt acetate in 0.1 M sodium acetate solution (pH 6) at a scan rate of 50 mVs^{-1} with a 3mm glassy carbon working electrode, a platinum wire as a counter electrode, and a Ag/AgCl (with 3 M KCl aqueous solution) reference electrode. B) Linear sweep voltammetry of 1 mM cobalt acetate in 0.1 M sodium acetate solution (pH 6); scans were taken using fresh glassy carbon electrode (blue), and a previously used electrode for several consecutive CV scans; 25 cycles (red), 50 cycles (black), and 100 cycles (green), in the range 0-1.3 V. The scan rate was 50 mV /s.

The addition of TCA ligand in 2:1 ratio to the cobalt ions resulted in a significant change in the electrochemical properties. Two equivalents of the ligand were dissolved in 0.1 M acetate buffer, followed by the addition of one equivalent of cobalt acetate. Directly after mixing, the cyclic voltammograms of Co-2TCA system showed an irreversible oxidation peak with initial current ~ 121 μA at 1.3 V (*vs.* Ag/AgCl electrode) (Figure 3A). As shown in the CVs, on subsequent 100 scans the catalytic current increases by ~ four folds suggesting the formation of a catalyst film on the electrode surface. After one hundred CV scans, the current reached to a measured value of 403 μA at 1.30 V corresponding to a current density of 5.75 mA/cm^2 (at pH 6), also the onset potential reached a value of 1.03 V (corresponding to an overpotential of 360 mV). This current density is much higher than those reported recently for

Co(II)-based catalyst for water oxidation that was deposited on FTO electrodes, showing a current density of < 1 mA/cm^2 at 1.5 V (*vs*. Ag/AgCl) in pH 7 phosphate buffer, at the same scan rate (50 mV/s).[21] In addition, it is favorable to compare with other excellent reported water oxidation catalysts. For example, the highly efficient cobalt carbonate (Co-Ci) film generated from cobalt (II) in neutral bicarbonate buffer, which showed a current density of 4.1 mA/cm^2 using GCE at 1.3 V (*vs.* Ag/AgCl) but at pH 7.[22] To check any possibility of ligand oxidation under the operating conditions, CV in the absence of cobalt acetate with the "TCA" ligand only in acetate buffer (pH 6) showed only double layer charging currents, with no significant Faradaic component (Figure 3A). While in some other case where mononuclear cobalt complexes with organic ligands decomposed to give nanoparticles in the photocatalytic water oxidation systems, the organic ligand suffered an electrochemical oxidation at potential lower than 1.0 V (*vs.* SCE) under similar operating conditions.[23]

Linear sweep voltammetry (LSV) was used to confirm the catalyst film growth *via* screening the catalytic current after several successive CV scans. For freshly polished GC electrode, LSV showed an oxidative wave with an onset potential of ~1.1 V (*vs.* Ag/AgCl) and wave catalytic current of 106 µA at 1.3 V. As the number of CV scans increases, the oxidation wave increases to 5-folds in magnitude and shifted to lower onset potentials after the first 100 CV scans (Figure 3b). Since the catalytic oxidation wave has increased over time, the initial catalyst cannot be the most active catalyst and might be converted to another more active form. An equilibrium between monomer diaqua cobalt complex **1** and oligomer/polymer or other molecular species that can be genrated under the external potential can account for the film formation. Moreover, the current cross-over observed in the first cycle of CVs at the on-set potential, in which the catalytic wave of anodic scan showed higher current than the reverse scan, presumably due to the re-solvation of the deposited film.

Several obtained data support the point that the deposited film from Co-2TCA catalytic system is a molecular cobalt specie rather than oxide/hydroxide film formation. The *in-situ* generated complex maintains a high hydrolytic stability and solubility (with concentrations up to 2 mM) in acetate solution (pH 6-8), as confirmed by UV-Vis spectroscopy and electrochemical measurements. UV-Vis spectroscopy did not show any change for aged catalyst in acetate solution for one month from a freshly mixed one. LSV for a freshly mixed and one-month aged solution were also identical. This confirms that the most active form of the catalyst is formed on applying the potential and not because of decomposition of the complex under operating conditions such as pH, aqueous hydrolysis, *etc*. This is different from some other catalytic systems based on cobalt polyoxometallates where nanoparticles formed directly after dissolving in buffer solutions.[13b] After one-hundred CV scans the electrode was removed from the catalyst solution and rinsed thoroughly with deionized water. The CV in catalyst free acetate buffer shows a clear drop in the catalytic current. This can be interpreted as, in the beginning a film is formed on the electrode surface with continuous scanning due to an equilibrium between the solution species and the surface species. Then, in catalyst free acetate buffer, this equilibrium is subjected to change and the film re-dissolves in the buffer solution resulting in the clear drop in the catalytic current after several CV scans as shown in Figure S8A.[24] Thereafter, under the same conditions, linear sweep voltammetry displayed a decrease in the magnitude of the catalytic current by *ca*. 5-folds and shifted to higher onset potential (Figure S8B). While in case of cobalt acetate a rinsed electrode in buffer alone shows the same features as seen in cobalt acetate solution; however no signals are present after polishing.

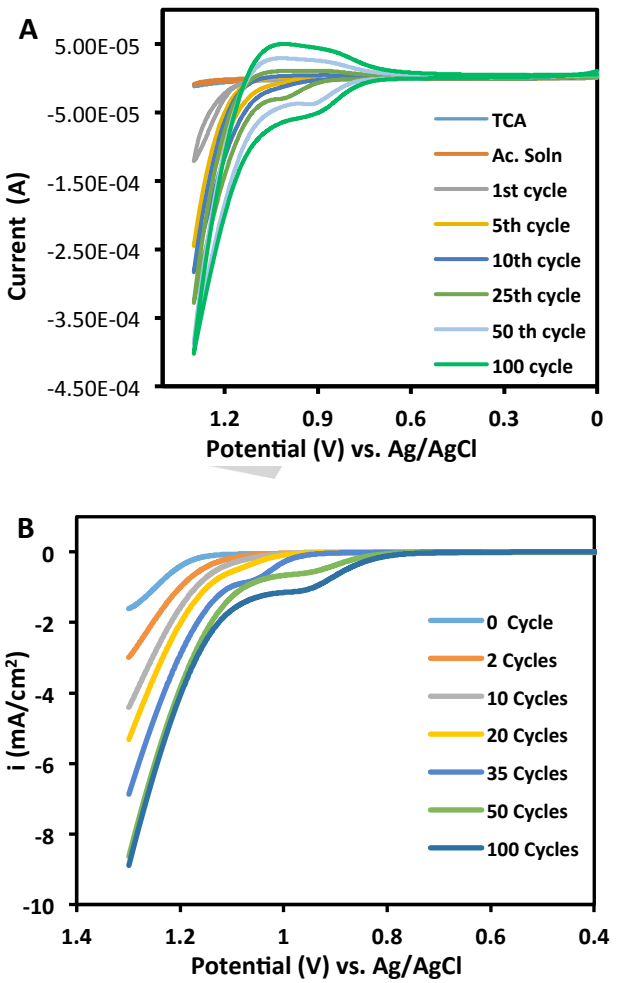

Figure 3. Electrochemical response of Co-2TCA under different experimental conditions. (A) 100 consecutive CV scans were performed for an aqueous 1 mM Co-2TCA solution in 0.1 M acetate buffer, pH 6, scan rate = 50 mV/s (Cycle 1 (blue), 5 (green), 10 (red), 25 (pink), 50 (brown) and 100 (black)). (B) Linear sweep voltammetry of 1 mM Co-2TCA in 0.1 M sodium acetate solution (pH 6); scans were taken using fresh glassy carbon electrode (blue), and a previously used electrode for several consecutive CV scans ; 5 scans (brown), 25 scans (green), 50 (pink), and 100 scans (black), in the range 0-1.3 V.

Using highly oriented pyrolytic graphite electrode (HOPG) (basal plane), the *in-situ* generated complex shows different electrochemical features. Cyclic voltammograms showed a quasi-reversible oxidation wave at 0.75 V that is assigned to $Co^{III/II}$ oxidation and an irreversible catalytic wave with an onset potential of ~1.05 V reaching an initial current ~ 161 µA at 1.3 V (*vs.* Ag/AgCl electrode) (Figure 4A). In differential pulse voltammogram (DPV) the peak of $Co^{III/II}$ appears clearly at 0.668 V (Figure 4B). Remarkably, the catalytic film electrodeposition on HOPG electrode was slower compared with a GC electrode, as the wave current amplified by 50 % after 25 CV cycles compared to 250% in case of GCE. This catalytic current of HOPG-film declined within 20 CV scans when used in catalyst free acetate buffer due to the film dissolution in the aqueous medium (Figure S9).

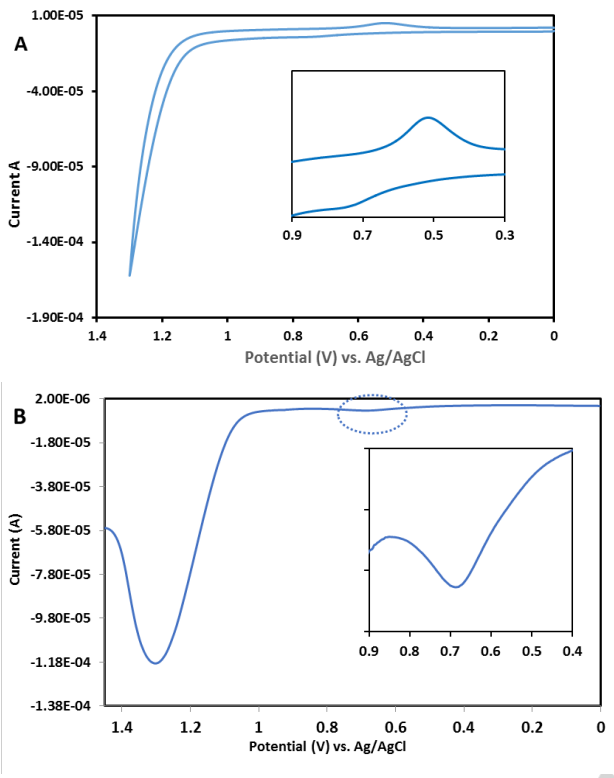

Figure 4. Electrochemical response; CV (A), DPV (B) of 1 mM Co-2TCA solution in 0.1 M acetate buffer, pH 6 using highly oriented pyrolytic graphite electrode (basal plane), scan rate = 50 mV/s.

To get a more comprehensive insight into the electrochemical behavior of the catalytic system, the dependence of the onset potentials on the pH was investigated in the pH range of 4.5-9.0. In the pH range 5.5-7.0, the onset of catalysis is shifted to higher potentials as the pH is lowered. The onset potential *vs.* pH plot shows a typical Nernstian behavior with 60 mV per pH shift, revealing that the one-electron oxidation is accompanied by the transfer of one proton (PCET) that is ascribed to the $[Co^{IV}=O]/[Co^{III}-OH]$ redox couple. At higher pH values (7.0 < pH > 8.7) the oxygen onset potential remains constant. This contrasts with the shift of approximately 60 mV/pH unit for the oxygen onset potential, which means that the electron transfer step is not coupled to proton transfer.[25] At pH>9, the onset potential shifts to higher value and the catalytic current for the water oxidation reaction decreases to more than 65 % of its value at pH 8.7 which is due to the decomposition of the catalyst under this basic conditions and the formation of cobalt bydroxide precipitate (Figure S10). Below pH 5.5 a large positive shift in the onset potential and diminished current density is observed.

Initial investigation of the deposited catalyst film on the glassy carbon electrode surface after 100 CV cycles using Raman spectroscopy showed two strong peaks at 2654 and 2910 cm^{-1}, and another weak peak at 3239 cm^{-1} (Figure 5a). These peaks correspond to C−H aliphatic/aromatic stretching vibrations which cannot arise from cobalt oxide film. Interestingly, the band appears at 3479 cm^{-1} fits to O−H stretching vibration of cobalt-coordinated aqua ligand. The relatively low feature that is observed in the range 544-712 cm^{-1} for Co–O bond which is what would have been expected if the Co were present as a metal organic film rather than being a cobalt oxide.[26] Moreover, the weak band in the range 302-575 cm^{-1} can be ascribed to Co-N bond from the metal complex.[27]

SEM of the electrodeposited catalytic film on a glassy carbon electrode showed complete coverage of the electrode surface, with a uniform film distribution across the surface. Notably, the high energy (~15 keV) incident electron beam resulted in burning of the deposited film indicating the organometallic nature of the film (Figure 5). Energy dispersive X-ray spectroscopy (EDX) revealed that the deposited catalytic film contained Co, O and C with an approximate Co:O ratio of 1:2.59. This high oxygen to cobalt ratio cannot be justified based on cobalt oxide structures such as CoO or Co_3O_4 where oxygen content is lower than cobalt. While in a molecular film of the complex, the Co:O ratio is calculated to be 1:2 which come close to the observed value. Moreover, the absence of any traces of sodium ions from the buffer solution in the deposited film strongly supports the molecular identity of the film. In contrast, for CoOx catalyst films, cations from the buffer solution typically Na and K are commonly observed in the film structure.[13b, 20, 28] The low ratio of detected nitrogen content by EDX might be attributed to the low sensitivity of this method to the surface composition (Figure S11).[29] EDX of the deposited film in case of ITO electrode gave an evidence for carbon incorporation in the catalyst film.

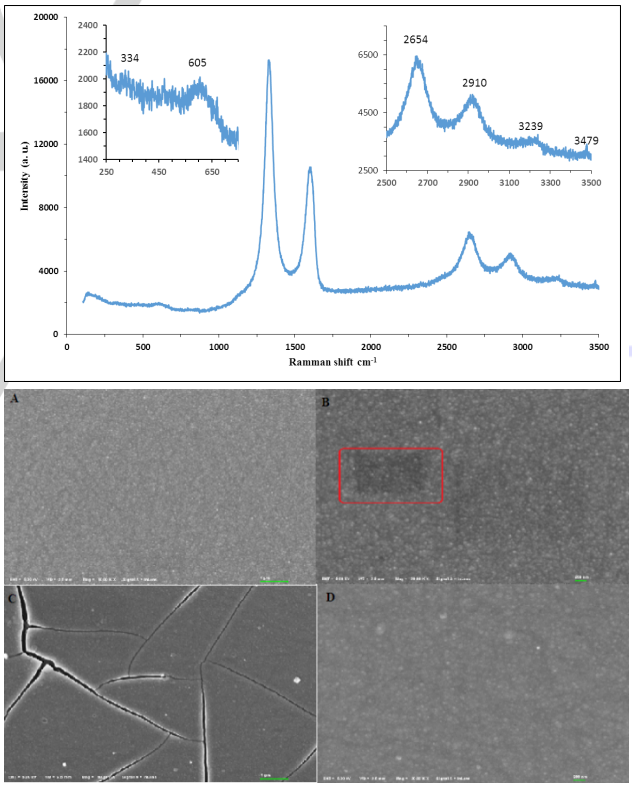

Figure 5. Raman spectrum (top) and FE-SEM of the deposited film on glassy carbon electrode (bottom); after 100 CV scans in the range 0-1.3V versus Ag/AgCl electrode with scan rate = 50 mV/s (A, B), after 1 h electrolysis (C, D) at 1.2 V versus Ag/AgCl electrode, of an aqueous 1 mM Co-2TCA solution in 0.1 M acetate buffer (pH 6).

For further characterization and in order to confirm the molecular identity of the deposited catalytic active film, we used an ITO electrode with larger surface area (0.5 cm^2) in controlled potential electrolysis experiment. After 11 h of electrolysis at 1.2 V (vs. Ag/AgCl), transparent brownish film of ~ 400 nm thickness was formed on the ITO electrode (Figure 6). The elemental

composition of the post-electrolysis ITO electrode and the valence states of metal elements were studied using X-ray photoelectron spectroscopy (XPS) analysis. The survey spectra of XPS recorded for the catalyst film indicated the presence of N-1s, C-1s, O -1s, and Co-2p peaks along with In and Sn from the electrode surface as shown in Figure 6. The high resolution XPS of cobalt showed two major peaks at 780.9 eV and 796.5 eV corresponding to Co $2p_{3/2}$ and Co $2p_{1/2}$, respectively. The absence of broad satellites (shake-up peaks) along with $Co2p_{1/2}$–$2p_{3/2}$ spin–orbit level energy spacing (~15.5 eV) supports the presence of low-spin Co(III).[30] XPS signals at 60 eV and 102 eV also consist with the presence of Co 3s and Co 3p.

The C1s core level spectrum displayed several peaks due to different functionalized carbons. The spectrum suggests the presence of C=C, C-C, C-N and COO in the deposited film as observed in the peaks at 284.5, 285.2, 286.6, and 288.5 eV, respectively. Remarkably, no C1s peak corresponding to carboxylic carbon (-COOH) appeared in the spectrum, indicating the absence of free ligand.[31] This rules out the ligand co-deposition with a metal oxide film and confirms the ligand coordination to the cobalt ion in the formed catalyst film. This C1s spectrum differs from the case of using cobalt acetate only in acetate buffer where two peaks at 285.1 eV and 288.3 eV represented the ionization of the carbon 1s core level of the methyl and carboxylate carbon from the acetate ion.[20]

The O1s peaks of the cobalt oxides Co_3O_4 and CoO nanoparticles are described to appear in the range of 529.4 – 530.3 eV.[32] While, deconvolution of the O1s peak gives three contributions at 531.8, 534.5, 535.5 eV, which is in a higher binding energy region compared with those of lattice oxygen O^{2-} from cobalt oxides. This result clearly shows that no persistent oxide layers are formed at any stage of the catalytic cycle. In addition, based on their binding energy values these peaks are assigned to O=C, O-C=O, and OH from a molecular catalytic film. The N1s XPS spectrum was deconvoluted into three major components at 399.2, 400.2 and 401.4 eV. The two peaks at high binding energy (400.2 and 401.4 eV) are assigned to free nitrogen atoms from the triazole structure.[33] Shift in binding energy of metal bounded N has been reported in the literature causing this peak to shift to lower binding energy ~399.2 eV.[34] Consequently, the third nitrogen atom from the triazole moiety also preserves its coordination to the cobalt ion in the deposited film.

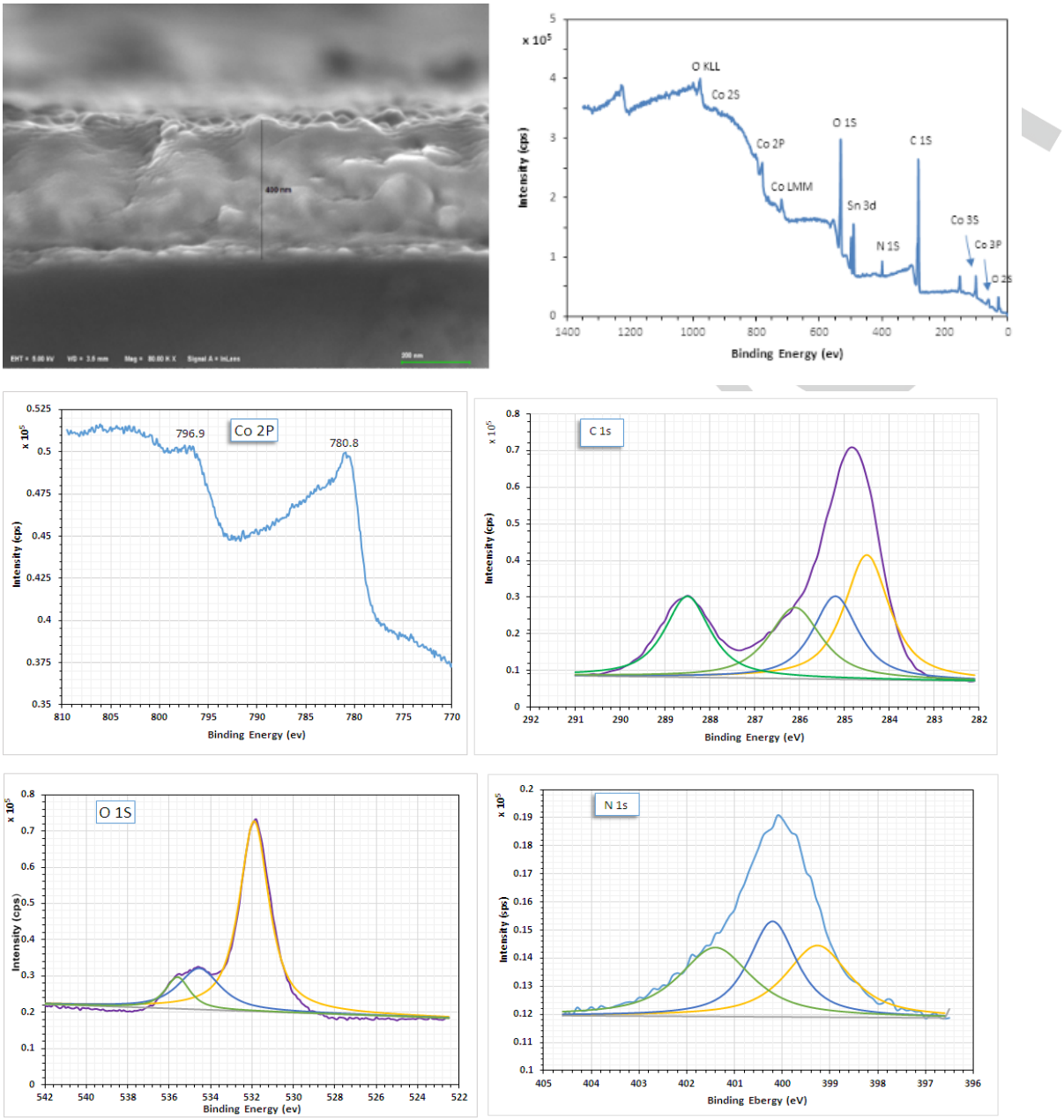

Figure 6. FE-SEM (top left), XPS survey (top right), and high-resolution scan for Co2p, C1s, O1s and N1s regions (bottom); of the deposited film on ITO electrode after 11 h of controlled potential electrolysis at 1.2 V (vs. Ag/AgCl), in acetate buffer (pH 6).

Another very conclusive evidence of the organometallic nature of the formed film was gained by dissolving the film in organic solvents. First trials to dissolve the brown film deposited on ITO electrode in organic solvents such as chloroform, methanol, ethanol, and acetone failed. Interestingly, using the same deposited catalyst film in a complex free acetate buffer in bulk electrolysis resulted in leaching of the film from the electrode surface into the aqueous solution. This brownish material was found to be soluble in organic solvents such as chloroform and ethanol. FT-IR of the dissolved film in chloroform matched well with the isolated product from the photochemical water oxidation experiment, using $Ru(bpy)_3^{2+}$ as photosensitizer and persulfate as the sacrificial electron acceptor (that is well characterized and discussed in details further)(Figure 7).

FT-IR spectra of the brown film separated after bulk electrolysis shows clear indications of the metal-organic nature of the deposited film. While the as-synthesized cobalt complex show a broad band in the range of 2880-3470 cm^{-1} for the coordinated water with superimposed weak peaks at 2852, 2918, and 3161 cm^{-1} assigned to C_{sp3}–H symmetric and asymmetric and C_{sp2}–H stretching vibrations. In addition, there are strong stretching frequencies at 1598, 1554, 1444, 1384, and 1062 cm^{-1} assigned to $C{=}O_{str}$, $C{=}C_{str}$, CH_{3bend}, and $C{-}O_{str}$ features, respectively. The post-electrolysis/photocatalysis separated brown powder showed a similar pattern compared with as-synthesized complex with a slight shift in some peaks. The aliphatic C-H stretching vibrations, from methyl groups, can be clearly seen as strong peaks at 2848, 2929, and 2952 cm^{-1}

together with a weak peak at 3200 cm^{-1} due to the aromatic C-H_{sp2} stretching vibrations. Moreover, there are weak to strong peaks at 1635, 1593, 1460, 1375, 1263 and 1062 cm^{-1} assigned to $C{=}O_{str}$, $C{=}C_{str}$, C=N, CH_{3bend}, and $C{-}O_{str}$ features, respectively. It is worth noting that the broad band in the O−H region of the complex was replaced by a weak sharp peak in case of the post-electrolysis film.

To further explore the structure of the cobalt species deposited on the working electrode, the brown film formed in bulk electrolysis experiment was analyzed by high-resolution electrospray ionization mass spectrometry (HR ESI-MS). The post-electrolysis film analysis confirmed the existence of complex **1** at m/z+ = 542.10999 which fits well with the calculated value of m/z+ = 542.10889 ($Co(TCA)_2{-}H_2O{+}Na^+$). The same value was observed for the as-synthesized catalyst. However, we cannot exclude the formation of some new molecular species since the ESI-MS spectrum of the film exhibited some new peaks compared to the as-synthesized complex (Figure S12). At the same time, the deposited film was free from any uncoordinated ligand (m/z = 231) or cobalt aqua ions ($[Co(H_2O)_6]^{2+}$ (m/z = 167).

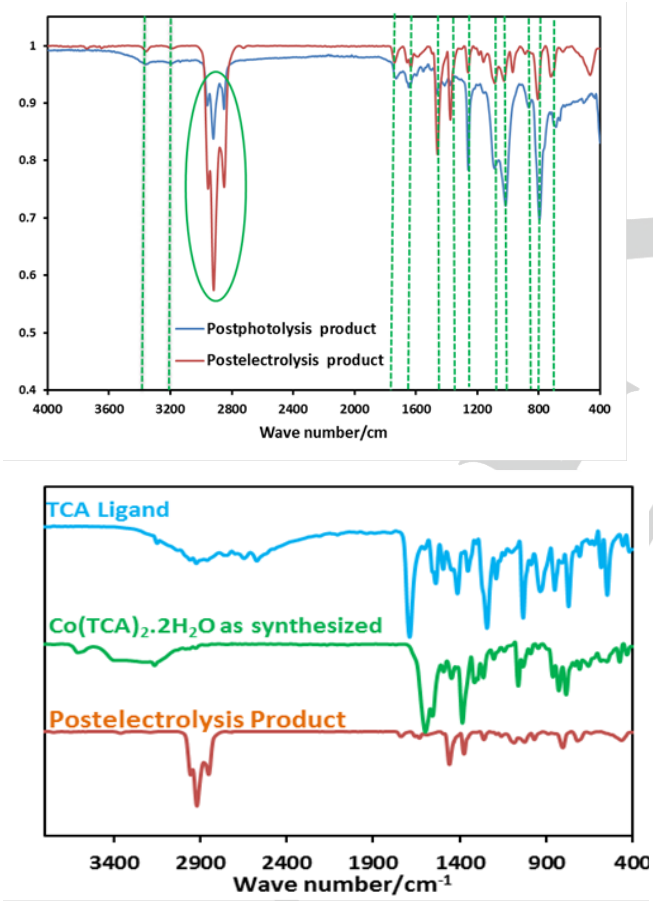

Figure 7. FT-IR of the post-electrolysis and post-photocatalysis product (upper) and FT-IR comparison of the ligand, the complex, and the post electrolysis product (lower).

Controlled potential electrolysis (CPE) for 11 hours in a one-compartment cell using the *in-situ* generated complex did not result in any metal deposition on the counter platinum electrode while in case of cobalt acetate a black deposition was clearly observed on the counter electrode. Optical spectra of the solution after 11 hour of electrolysis at 1.2 v (*vs.* Ag/AgCl) indicated only about 8% decrease in the catalyst concentration which is expected due to the deposition of cobalt complex on the working electrode surface (Figure S13). Hence, the catalyst is still present after a long period of electrolysis. Moreover, the catalyst displayed a linear dependence of catalytic current on the catalyst concentration (Figure S14). This dependence is unlikely to be caused by a surface adsorbed species because similar catalysis is observed with three different electrode materials (GC, HOPG, and ITO). Furthermore, the *in-situ* generated cobalt complex discloses a catalytic current dependence on the electronic structure of the complex. Thus, using the electron deficient bidentate ligand 1-phenyl triazole-4-carboxylic acid leads to a decrease in the catalytic current of more than 50% and an increase of the water oxidation overpotential compared with the use of TCA (Figure S15). Llobet and coworkers very recently reported similar findings in their mononuclear Cu-based WO catalyst where they demonstrated that as the electron-donating capacity at the aromatic ring increases, the overpotential drastically reduces.[35]

The apparent catalytic currents for water oxidation prompted us to examine controlled potential electrolysis catalyzed by the *in-situ* generated complex $Co(TCA)_2.2H_2O$. The experiment was carried out at a fixed potential (1.2 V *vs.* Ag/AgCl) in 0.1 M acetate electrolyte (pH 6.0) containing 1 mM of catalyst. The system shows a very stable oxygen evolution current density of ~2.0 mA/cm^2, and a transparent brown film was observed on the ITO after 2 h of electrolysis (Figure S16). The electrocatalyst remains very active during extended periods of CPE over 11 h with high current density for oxygen evolution (Figure 8). During electrolysis, gas bubbles were clearly observed, and these bubbles have been confirmed as oxygen molecules by gas chromatography. No apparent O_2 evolution current was observed on the bare ITO immersed in catalyst free acetate buffer. After 11 h of CBE, the electrode was transferred to a catalyst free acetate electrolyte of pH~7.5 to show a stable current density of 2.7 mA/cm^2.

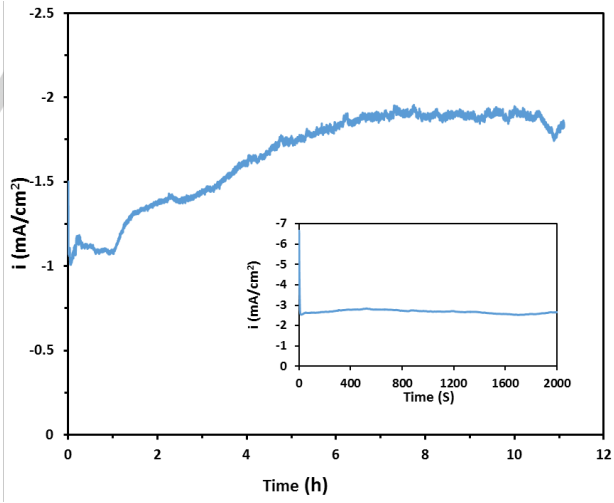

Figure 8. Long-term controlled-potential electrolysis of ITO electrode in 0.1 M acetate solution (pH=6.0) containing 1 mM Co-TCA at 1.2 V (vs. Ag/AgCl). The inset shows CBE using the deposited film on the ITO surface in catalyst free acetate solution of pH 7.5.

Photochemical water oxidation

The catalytic efficiency of the *in-situ* generated complex $Co(TCA)(OH_2)_2$ for visible light-driven water oxidation was studied by using $[Ru(bpy)_3]Cl_2$ as the photosensitizer (PS) and $Na_2S_2O_8$ as the sacrificial oxidant, in a sodium acetate solution (pH 7.0) under visible light irradiation (λ > 420 nm). Oxygen

evolution was monitored using gas chromatography with a thermal conductivity detector (GC-TCD). Under photocatalysis, oxygen evolution starts and throughout the first hour, the amount of O_2 increases linearly reaching ~ 90 µmole of oxygen in the gaseous phase after one hour of photocatalysis corresponding to a TON of 90 (mol O_2/mol **1**). The oxygen production stops around one hour after the start of photoirradiation due to $[Ru(bpy)_3]^{2+}$ degradation, as indicated by partial diminishing of the absorption peak at 450 nm (Figure S17).

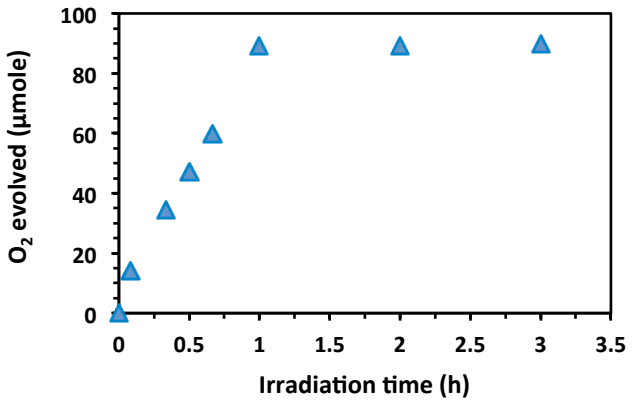

Figure 9. Plot of oxygen evolution *vs.* time for visible light-driven (>420 nm) water oxidation catalyzed by $Co(TCA)(OH_2)_2$ (100 µM), in aqueous acetate solution (0.1M, 10 mL; pH 7.5) containing $Na_2S_2O_8$ (10 mM) and $[Ru(bpy)_3]Cl_2$ (1 mM) under N_2.

Determination of the complex stability for water oxidation under the operating conditions such as aqueous medium, pH, oxidation potential, *etc.* is the first step in proving the molecular nature of the catalytic system. Subsequently, catalyst speciation or isolation and *ex-situ* characterization, where possible, could give further breakthrough about the active species during reaction. The molecular identity of the cobalt catalyst (**1**) was proven based on both *in-situ* and *ex-situ* catalyst characterizations. Firstly, a solution containing the *in-situ* generated complex $Co(TCA)(OH_2)_2$ (0.05 mM), 10 mol equiv. of $[Ru(bpy)_3]Cl_2$ and 20 mol equiv. of $Na_2S_2O_8$ in a acetate solution (pH 7.5) was subjected to electrospray ionization mass spectroscopy (ESI-MS) and after 3 hours of photoirradiation the solution was analyzed again using ESI-MS. The mass spectrum of the photoirradiated sample confirmed the exact molecular weight of the catalyst at m/z 553.41($Co(TCA)(OH_2)_2$-$2H^+$), the same as before photocatalysis, exist in the solution. This means that the catalyst is very stable under the photocatalysis conditions as it maintains its structure for long period of photocatalysis (Figure S18). No peak for free dissociated ligand was observed in the ESI-MS spectrum after photocatalysis, which would otherwise appear as at m/z = 231 corresponding to TCA. Besides, no peaks from cobalt aqua ions were detected.

Moreover, time-dependent dynamic light scattering (DLS) was used to rule out the formation of any cobalt species nanoparticles under photolytic conditions, above the limit of detection, while those catalyzed by cobalt acetate do produce particles which are presumably CoOx. Several samples of the photoirradiated catalyst solution were collected at different time intervals (till 2 hours) and no nanoparticles can be detected (Figures S19 and S20).

Since the *in-situ* characterization of the reaction solution before and after the photochemical water oxidation reaction, using ESI-MS suggesting the high stability of the cobalt catalyst and DLS analysis ruling out the formation of nanoparticles during the process. A second and conclusive step in distinguishing homogeneous and heterogeneous catalysis is the catalyst isolation and *ex-situ* characterization of any detected forms of the catalyst. Therefore, firstly a solution containing 0.1 mM of the catalyst 1, 1 mM of $[Ru(bpy)_3]Cl_2$ and 10 mM of $Na_2S_2O_8$ in a acetate buffer (0.1 M) at pH 7.5 was irradiated under visible light for two hours. After water evaporation at room temperature, the reaction residue was dissolved in chloroform. Providentially, both of TCA ligand and the cobalt complex $Co(TCA)_2.2H_2O$ are soluble in chloroform as independently tested. The chloroform solution was then analyzed by ESI-MS, ^{1}H-NMR and FTIR. ESI-MS of the post-photocatalysis isolated product revealed an identical mass spectrum to that of the as-synthesized complex, with the absence of any peak corresponding to the free ligand (Figure 10).

^{1}H-NMR of the free TCA ligand revealed two sharp peaks in the aliphatic region closely at 1.94 and 2.35 ppm which are equivalent to 6H and 3H, respectively, from the three methyl groups on the mesityl moiety. After coordination, in the as-synthesized cobalt complex $Co(TCA)_2.2H_2O$, these two peaks have clearly shifted to the right with an exchange of their peak positions. Thus, in the complex the two peaks appeared at 1.98 ppm (equivalent to 3H) and 2.10 ppm (equivalent to 6H), while the peaks in the aromatic region, which localize close to the cobalt ion, were not well-defined as the complex contains the paramagnetic Co(II) ion. Similarly, the peaks of the product isolated after photoirradiation are very analogous to those of the as-synthesized catalyst (Figure 10). The absence of any peaks from the dissociated ligand or its oxidation products along with retaining the integration ratio of the two peaks corresponding to the methyl groups, the same as in the as-synthesized catalyst, strongly support that the catalyst preserves its molecular identity under photocatalysis conditions. The ^{1}H-NMR spectrum of the post-photocatalysis product noticeably exhibited sharp resonances with slight change in the peaks' chemical shift which might be due to the complex oxidation to diamagnetic Co(III) analogue. The ligand oxidation products can be easily detected in ^{1}H-NMR, nonetheless ^{1}H-NMR did not detect any ligand dissociation or its oxidation products. Also, during the photochemical water oxidation mass spectroscopy could not detect any CO_2 gas which excludes the ligand decomposition under harsh photocatalysis conditions.

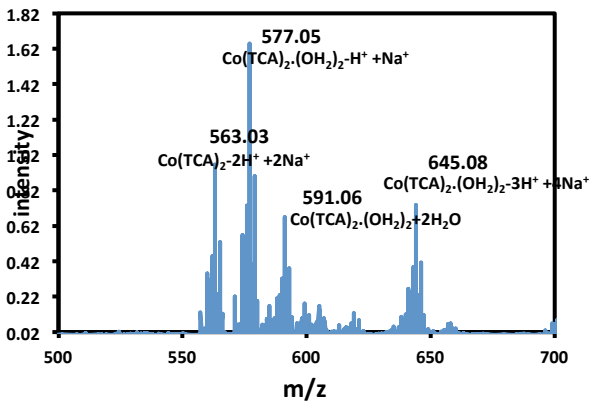

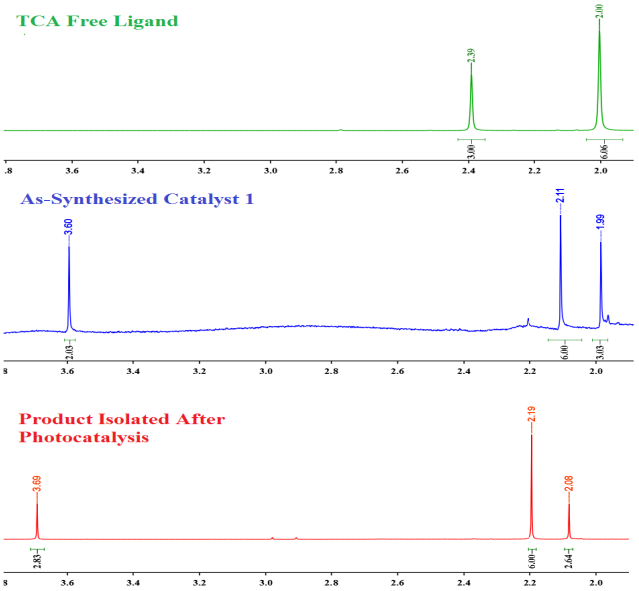

Figure 10. Characterizations of the product isolated after 2 h of photoirradiation; Conditions: $Co(TCA)(OH_2)_2$ (0.1 mM), 10 mol equiv. of $[Ru(bpy)_3]Cl_2$ and 100 mol equiv. of $Na_2S_2O_8$ in an acetate solution (pH 7.5) was photoirradiated with Xe-lamp at λ >420 nm for 2 h; A) ESI-MS, B) ^{1}H-NMR comparison of the free TCA ligand (Green), as-synthesized catalyst (Blue), and the isolated product after photocatalysis (Red).

DFT Calculations

For water oxidation an electrochemical potential of 1.23 eV per electron is required at pH=0.[36] Some possible catalytic cycles were modeled (**Figure 11**) and compared with the calculated performance of our complex with other possible water oxidation catalysts in a volcano plot (**Figure 12**).

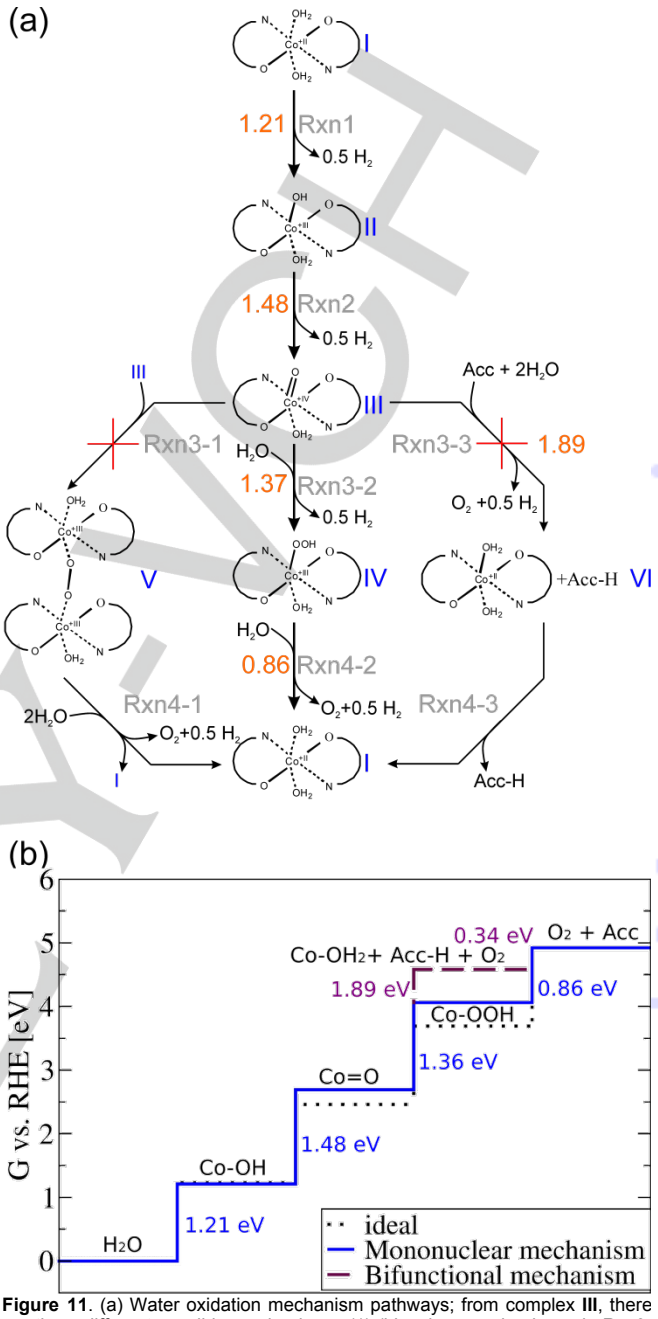

Figure 11. (a) Water oxidation mechanism pathways; from complex **III**, there are three different possible mechanisms: (1) (binuclear mechanism, via Rxn3-1 and Rxn4-1); (2) mononuclear mechanism (via Rxn3-2 and Rxn4-2); and (3) bifunctional mechanism (via Rxn3-3 and Rxn4-3) in which an Acceptor (Acc) has a co-catalytic role. (b) Stepwise representation of the water oxidation according to the mononuclear mechanism (following Rxn1, Rxn2, Rxn3-2 and Rxn4-2).

To elucidate the potential water oxidation mechanism DFT calculations were performed (see electronic supporting information for more details about the level of theory used). The mechanisms were studied considering only key intermediates reached through proton coupled electron transfers. The redox potentials were computed by taking advantage of the theoretical Normal Hydrogen Electrode (NHE) developed by Rossmeisl *et al.*[37] For convenience, we discuss our results with respect to the Reversible Hydrogen Electrode (RHE), of which the potential does not change with the pH. In Figure 11a, the three most

common potential water oxidation mechanisms which adds a pH correction to 59 meV/pH. Accordingly all redox potentials discussed here become pH independent. The first two reaction steps (Rxn1 and Rxn2) comprise the subsequent abstraction of H^+/e^- couples resulting in the formation of Co^{+III}-OH hydroxo and Co^{+IV}=O oxo intermediates. In the present set of calculations we find a potential of 1.21 eV and 1.48 eV to be required for these oxidations steps (versus RHE). The Co^{+IV}=O species (**III** in Figure 11a) correspond to a branching point from which O-O bond formation can proceed through a variety of different mechanisms. The most common reaction paths summarized in the literature are the bi-nuclear path[38] (Rxn3-1), the mononuclear path[37, 39] (Rxn3-2) and the recently discovered bi-functional path[40] (Rxn3-3). Each of the three mechanisms is characterized by different structural requirements. The bi-nuclear mechanism[41] requires the presence of two easily available adjacent Co sites to proceed. Due to the mono-nuclear nature of the complex the only possibility to fulfill this requirement is the co-operative interaction between two pre-oxidized complexes resulting in the formation of a Co-O-O-Co peroxo bridge between them. The rather large π-π-stacking distance of 5 Å – 6 Å, however, renders this possibility unlikely. Despite this unfavorable steric hindrance it is still not impossible to form such a bridge, at the cost of a considerable activation barrier. However, the fact that the complex still displays considerable current density even after being placed on an ITO electrode where no longer freely moving Co=O moieties are available prompts us to exclude this mechanism.

This renders the nucleophilic attack of a water or OH^- molecule the most likely path to O-O bond formation (Rxn3-2 and Rxn4-2). Assuming this path, the nucleophilic attack of water is generally assumed to result in the formation of a Co^{+III}-OOH intermediate under abstraction of a H^+/e^- couple (Rxn3-2).[37, 42] Following this mechanism a potential of 1.16 eV is required for O-O bond formation followed by the release of O_2 requiring a potential of 0.86 eV. Thus, the oxidation of Co-OH to Co=O appears, with an overpotential of 0.25 eV, to be potential determining (Figure 11b).

Recently also a bi-functional mechanism for the nucleophilic O-O bond formation step has been proposed in the heterogeneous electrochemistry community (via Rxn3-3).[41] In contrast to the classical mono-nuclear mechanism the O-O bond formation is here assumed to happen in a concerted reaction step comprising the nucleophilic attack of a water molecule, the abstraction of the H^+/e^- couple and the transfer of the second hydrogen to an adjacent hydrogen acceptor unit Acc (Figure 11a). This mechanism allows for the direct formation of O_2 and avoids the formation of Co-OOH (Rxn3-3).

$$Co{=}O + 2H_2O + Acc \rightarrow [Co\text{-}H_2O + Acc\text{-}H] + O_2 + 0.5\ H_2 \quad \text{(Rxn3-3)}$$

A prerequisite for this mechanism is however the availability of a reasonably reactive H acceptor in close vicinity to the active site. In the present complex only a nitrogen in the triazole ring or a second Co=O could act as co-catalyst. The former can be excluded since the triazole ring has a redox potential of 0.34 eV vs. RHE, rendering it a poor H acceptor. Indeed the O-O bond formation would, with a redox potential of 1.89 eV vs RHE, become the potential determining step. Similarly also the H transfer to a Co=O, provided it is accessible under reaction conditions, would not change the energy landscape as this would not avoid the potential determining reaction step Rxn2. Additionally it would add an equally unfavorable reaction step Rxn4-3 for the recovery of the Co=O acceptor unit. Thus, the bi-functional mechanism can be excluded for the present system.

Based on the energetics of the key intermediates a comparison of the catalyst's activity with state of the art molecular and solid state water oxidation catalysts can be performed using a volcano plot.[39, 43] Volcano plots are drawn by plotting the activity (here the overpotential η) at the y-axis and a descriptor for the activity (here the Rxn2) at the x-axis. The plot is a graphical representation of Sabatier's principle which states that for the best possible catalyst all reaction steps display comparable energetics.[44] These ideal catalysts are found at the top of the volcano while less ideal materials are shifted away from the top and appear either on the left branch of the volcano if the intermediates are bound too strongly or at the right branch in case they are too unstable. Details on the construction and interpretation of volcano plots can be found in the references[43a, 43b] and the SI.

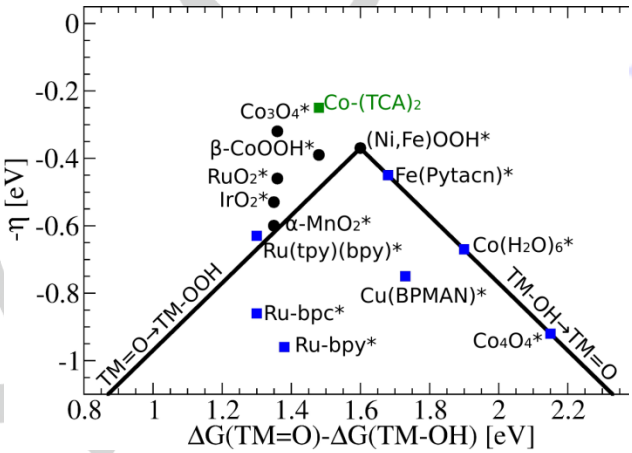

Figure 12. A DFT based volcano plot relating the theoretical limiting over-potential of various transition metal (TM) complexes and oxide surfaces to general ORR reactivity trends; RuO_2, IrO_2, Co_3O_4 (ref.[39]); α-MnO_2 (ref.[45]); β-CoOOH (ref.[46]); (Ni,Fe)OOH (ref.[47]); $Co(H_2O)_6$ (ref.[48]); Co_4O_4 cubane (ref.[49]); Fe(Pytacn) (ref.[50]); Ru(tpy)(bpy) (ref.[51]); Cu_2(BPMAN) (ref.[52]); Ru-bpc and Ru-bpy (ref.[42]); $Co(TCA)_2$ (this paper).

Let us begin the discussion of the volcano plot shown in Figure 12 by considering the general shape of the OER volcano. The most prominent feature is the volcano's peak, which is placed at a reaction free energy of Rxn2 of 1.6 eV rather than the thermodynamic potential of 1.23 eV. This is a direct result of the constant energy difference of 3.2 eV which has been observed for a large number of very different systems ranging from transition metal oxides to transition metal doped graphenes.[39, 41b, 53] With a theoretical overpotential of only 0.25 eV and a Rxn2 reaction free energy of 1.48 eV our catalyst falls close to the top of the volcano slightly shifted to the left branch of the volcano where catalysts with too stable intermediates are placed. This resembles the excellent performance of the complex observed experimentally. To which extend minor improvements through destabilization of the intermediates with less electron donating ligands can be achieved is unclear considering the computational uncertainties associated with the modeling of transition metal complexes.[54] Furthermore, it is equally active as state of the art Dimensionally Stable Anodes (DSA) used in industrial water oxidation which rely on IrO_2 and RuO_2[39, 55] and outperforms many of the recently discovered homogeneous water oxidation catalysts based on abundant transition metal oxides.[39, 42, 46-52, 56]

Conclusions

In summary, we have demonstrated that the *in-situ* generated $Co(TCA)_2.2H_2O$ is an active catalyst for both the photochemical and electrochemical water oxidation reaction. In electrochemical investigations, the catalyst was found to self-assemble to a catalyst film on the surface of different electrodes such as GC, HOPG, and ITO electrodes. The film was proved not to be cobalt oxide/hydroxide as normally happen but for the first time, a molecular cobalt complex incorporating the original ligand ligated to the cobalt. The film was evidenced based on its SEM, Raman, FTIR, and XPS spectra results along with its physical properties. Similar results were observed with copper(II)/6,6-dihydroxy-2,2-bipyridine catalytic system when used for electrochemical water oxidation, where a deposit was observed on the electrode during electrolysis experiments and it was demonstrated that this film is oligomer or polymer of the copper complex instead of copper oxide.[24] Moreover in the photochemical WO, the catalytic activity of the complex competes with some of the best WOCs reported so far in terms of stability and TON. The molecular identity of the catalyst in the photocatalysis process was evidenced based on ESI-MS, DLS, FTIR, and ^{1}H-NMR characterizations. The proof of the high stability of the *in-situ* generated complex and its high catalytic activity under neutral conditions which is based only on a bidentate ligand, shed light on the ability of small ligands, instead of a pre-synthesized polydentate ligands, to stabilize cobalt ions in lower as well as higher oxidation states. Furthermore, DFT calculations predict a mono-nuclear oxidation mechanism and show that this $Co(TCA)_2.2H_2O$ catalyst lies very close to the top of the theoretical volcano plot. Based on these computational results, we are confident that small modifications of this type of catalyst can lead to a superb – easily synthesized – industrial water oxidation catalyst.

Acknowledgements

The authors are grateful to the State Key Lab of Advanced Technology for Materials Synthesis and Processing for financial support (Wuhan University of Technology). M.V. acknowledges funding from the Scientific Research-Foundation Flanders (FWO) for a postdoctoral fellowship. F.V. acknowledges the Chinese Central Government for an “Expert of the State” position in the program of “Thousand talents”.

Keywords: water splitting, electrochemical/photochemical water oxidation, metal-organic film, *in-situ* generation.

[1] Y. Umena, K. Kawakami, J.-R. Shen, N. Kamiya, *Nature* **2011**, *473*, 55-60.

[2] a) M. D. Kärkäs, O. Verho, E. V. Johnston, B. r. Åkermark, *Chem. Rev.* **2014**, *114*, 11863-12001; b) J. D. Blakemore, R. H. Crabtree, G. W. Brudvig, *Chem. Rev.* **2015**, *115*, 12974-13005.

[3] a) L. Duan, Y. Xu, L. Tong, L. Sun, *ChemSusChem* **2011**, *4*, 238-244; b) D. G. Hetterscheid, J. N. Reek, *Angew. Chem. Int. Ed.* **2012**, *51*, 9740-9747; c) N. Kaveevivitchai, R. Zong, H.-W. Tseng, R. Chitta, R. P. Thummel, *Inorg. Chem.* **2012**, *51*, 2930-2939; d) L. Tong, A. K. Inge, L. Duan, L. Wang, X. Zou, L. Sun, *Inorg. Chem.* **2013**, *52*, 2505-2518; e) L. Tong, Y. Wang, L. Duan, Y. Xu, X. Cheng, A. Fischer, M. r. S. Ahlquist, L. Sun, *Inorg. Chem.* **2012**, *51*, 3388-3398; f) A. G. Walden, A. J. Miller, *Chem. Sci.* **2015**, *6*, 2405-2410; g) C. Wang, Y. Chen, W.-F. Fu, *Dalton. Trans.* **2015**, *44*, 14483-14493; h) Q. Zeng, F. W. Lewis, L. M. Harwood, F. Hartl, *Coord. Chem. Rev.* **2015**, *304*, 88-101.

[4] a) A. Lewandowska-Andralojc, D. E. Polyansky, C.-H. Wang, W.-H. Wang, Y. Himeda, E. Fujita, *Phys. Chem. Chem. Phys.* **2014**, *16*, 11976-11987; b) N. D. McDaniel, F. J. Coughlin, L. L. Tinker, S. Bernhard, *J. Am. Chem. Soc.* **2008**, *130*, 210-217; c) J. A. Woods, R. Lalrempuia, A. Petronilho, N. D. McDaniel, H. Müller-Bunz, M. Albrecht, S. Bernhard, *Energ. Environ. Sci.* **2014**, *7*, 2316-2328; d) M. Li, K. Takada, J. I. Goldsmith, S. Bernhard, *Inorg. Chem.* **2016**, *55*, 518-526; e) M. Navarro, M. Li, H. Müller-Bunz, S. Bernhard, M. Albrecht, *Chem. Eur. J. 2014,* **2016**, *22*, 6740-6745.

[5] a) M. A. Asraf, H. A. Younus, C. I. Ezugwua, A. Mehta, F. Verpoort *Catal. Sci. Technol.* **2016**, 6, 4271-4282 b) M. A. Asraf, H. A. Younus, M. Yusubov, F. Verpoort, *Catal. Sci. Technol.* **2015**, *5*, 4901-4925; c) C. Lu, J. Du, X.-J. Su, M.-T. Zhang, X. Xu, T. J. Meyer, Z. Chen, *ACS Catal.* **2015**, *6*, 77-83; d) Y. Zhao, J. Lin, Y. Liu, B. Ma, Y. Ding, M. Chen, *Chem. Commun.* **2015**, *51*, 17309-17312; e) D. Das, S. Pattanayak, K. K. Singh, B. Garai, S. Sen Gupta, *Chem. Commun.* **2016**, *52*, 11787-11790.

[6] a) S. M. Barnett, K. I. Goldberg, J. M. Mayer, *Nat. Chem.* **2012**, *4*, 498-502; b) Z. Chen, T. J. Meyer, *Angew. Chem. Int. Ed.* **2013**, *52*, 700-703; c) M.-T. Zhang, Z. Chen, P. Kang, T. J. Meyer, *J. Am. Chem. Soc.* **2013**, *135*, 2048-2051.

[7] a) W. A. Arafa, M. D. Kärkäs, B.-L. Lee, T. Åkermark, R.-Z. Liao, H.-M. Berends, J. Messinger, P. E. Siegbahn, B. Åkermark, *Phys. Chem. Chem. Phys.* **2014**, *16*, 11950-11964; b) E. A. Karlsson, B. L. Lee, R. Z. Liao, T. Åkermark, M. D. Kärkäs, V. S. Becerril, P. E. Siegbahn, X. Zou, M. Abrahamsson, B. Åkermark, *ChemPlusChem* **2014**, *79*, 936-950.

[8] a) B. Das, B.-L. Lee, E. A. Karlsson, T. Åkermark, A. Shatskiy, S. Demeshko, R.-Z. Liao, T. M. Laine, M. Haukka, E. Zeglio, *Dalton. Trans.* **2016**; 45, 13289-13293; b) W. C. Ellis, N. D. McDaniel, S. Bernhard, T. J. Collins, *J. Am. Chem. Soc.* **2010**, *132*, 10990-10991; c) J. L. Fillol, Z. Codolà, I. Garcia-Bosch, L. Gómez, J. J. Pla, M. Costas, *Nat. Chem.* **2011**, *3*, 807-813; d) B. M. Klepser, B. M. Bartlett, *J. Am. Chem. Soc.* **2014**, *136*, 1694-1697; e) B. Das, A. Orthaber, S. Ott, A. Thapper, *ChemSusChem* **2016**, *9*, 1178-1186; f) G. Panchbhai, W. M. Singh, B. Das, R. T. Jane, A. Thapper, *Eur. J. Inorg. Chem.* **2016**, *2016*, 3262-3268; g) B. Das, B.-L. Lee, E. A. Karlsson, T. Akermark, A. Shatskiy, S. Demeshko, R.-Z. Liao, T. M. Laine, M. Haukka, E. Zeglio, A. F. Abdel-Magied, P. E. M. Siegbahn, F. Meyer, M. D. Karkas, E. V. Johnston, E. Nordlander, B. Akermark, *Dalton. Trans.* **2016**, *45*, 13289-13293; h) C. Panda, J. Debgupta, D. D. Díaz, K. K. Singh, G. S. Sen, B. B. Dhar, *J. Am Chem. Soc.* **2014**, *136*, 12273-12282; i) Y. Liu, R. Xiang, X. Du, Y. Ding, B. Ma, *Chem. Commun.* **2014**, *50*, 12779-12782.

[9] a) D. Wang, G. Ghirlanda, J. P. Allen, *J. Am. Chem. Soc.* **2014**, *136*, 10198-10201; b) L. Wang, L. Duan, R. B. Ambre, Q. Daniel, H. Chen, J. Sun, B. Das, A. Thapper, J. Uhlig, P. Dinér, *J. Catal.* **2016**, *335*, 72-78; c) Y. Han, Y. Wu, W. Lai, R. Cao, *Inorg. Chem.* **2015**, *54*, 5604-5613.

[10] a) J. Suntivich, K. J. May, H. A. Gasteiger, J. B. Goodenough, Y. Shao-Horn, *Science* **2011**, *334*, 1383-1385; b) Z. Zhuang, W. Sheng, Y. Yan, *Adv. Mater.* **2014**, *26*, 3950-3955; c) R. D. Smith, M. S. Prévot, R. D. Fagan, Z. Zhang, P. A. Sedach, M. K. J. Siu, S. Trudel, C. P. Berlinguette, *Science* **2013**, *340*, 60-63; d) J. Masa, W. Xia, I. Sinev, A. Zhao, Z. Sun, S. Grützke, P. Weide, M. Muhler, W. Schuhmann, *Angew. Chem. Int. Ed.* **2014**, *53*, 8508-8512; e) L.-A. Stern, L. Feng, F. Song, X. Hu, *Energy Environ. Sci.* **2015**, *8*, 2347-2351.

[11] a) M. W. Kanan, D. G. Nocera, *Science* **2008**, *321*, 1072-1075; b) D. Wang, J. T. Groves, *Proc. Natl. Acad. Sci. USA* **2013**, *110*, 15579-15584; c) S. M. Barnett, K. I. Goldberg, J. M. Mayer, *Nat. Chem.* **2012**, *4*, 498-502; d) Z. Chen, T. J. Meyer, *Angew. Chem. Int. Ed.* **2013**,*125*, 728-731; e) M. Dincă, Y. Surendranath, D. G. Nocera, *Proc. Natl. Acad. Sci. USA* **2010**, *107*, 10337-10341; f) A. K. Poulsen, A. Rompel, C. J. McKenzie, *Angew. Chem. Int. Ed.* **2005**, *44*, 6916-6920; g) R. K. Hocking, R. Brimblecombe, L.-Y. Chang, A. Singh, M. H. Cheah, C. Glover, W. H. Casey, L. Spiccia, *Nat. Chem.* **2011**, *3*, 461-466; h) E. A. Karlsson, B.-L. Lee, T. Åkermark, E. V. Johnston, M. D. Kärkäs, J. Sun, Ö. Hansson, J.-E Bäckvall, B. Åkermark, Angew. Chem. Int. Ed. **2011**, 50, 11715 – 11718; i) M. Zhang, M.-T. Zhang, C. Hou, Z.-F. Ke, T.-B. Lu, *Angew. Chem. Int. Ed.* **2014**, *53*, 13042-13048; j) M. M. Najafpour, G. Renger, M. Hołyńska, A. N. Moghaddam, E.-M. Aro, R. Carpentier, H. Nishihara, J. J. Eaton-Rye, J.-R. Shen, S. I. Allakhverdiev, *Chem. Rev.* **2016**, *116*, 2886-2936; k) J. L. Fillol, Z. Codolà, I. Garcia-Bosch, L. Gómez, J. J. Pla, M. Costas, *Nat. Chem.* **2011**, *3*, 807-813; l) S. D. Tilley, M. Cornuz, K. Sivula, M. Grätzel, Angew. Chem. Int. Ed. **2010**, 49, 6405; m) M. D. Kärkäs, B. Åkermark, *Dalton Transactions* **2016**; n) K. S. Joya, Y. F. Joya, H. J. De Groot, *Adv. Energy Mater.* **2014**, *4*.

[12] a) V. Artero, M. Chavarot-Kerlidou, M. Fontecave, *Angew. Chem. Int. Ed.* **2011**, *50*, 7238-7266; b) C.-F. Leung, S.-M. Ng, C.-C. Ko, W.-L. Man, J. Wu, L. Chen, T.-C. Lau, *Energy Environ. Sci.* **2012**, *5*, 7903-7907; c) B. M. Hunter, H. B. Gray, A. M. Müller, *Chem. Rev.* **2016**. DOI: 10.1021/acs.chemrev.6b00398

[13] a) J. J. Stracke, R. G. Finke, *ACS Catal.* **2014**, *4*, 909-933; b) J. J. Stracke, R. G. Finke, *J. Am. Chem. Soc.* **2011**, *133*, 14872-14875.

[14] V. Artero, M. Fontecave, *Chem. Soc. Rev.* **2013**, *42*, 2338-2356.

[15] a) Q. Yin, J. M. Tan, C. Besson, Y. V. Geletii, D. G. Musaev, A. E. Kuznetsov, Z. Luo, K. I. Hardcastle, C. L. Hill, *Science* **2010**, *328*, 342-345; b) H. Y. Wang, E. Mijangos, S. Ott, A. Thapper, *Angew. Chem. Int.*

Ed. **2014**, 53, 14499; c) J.-W. Wang, P. Sahoo, T.-B. Lu, *ACS Catal.* **2016**, 5062-5068.

[16] A. M. Ullman, Y. Liu, M. Huynh, D. K. Bediako, H. Wang, B. L. Anderson, D. C. Powers, J. J. Breen, H. D. Abruña, D. G. Nocera, *J. Am. Chem. Soc.* **2014**, *136*, 17681-17688.

[17] a) T. Abe, K. Nagai, S. Kabutomori, M. Kaneko, A. Tajiri, T. Norimatsu, *Angew. Chem. Int. Ed.* **2006**, *45*, 2778-2781; b) D. K. Dogutan, R. McGuire Jr, D. G. Nocera, *J. Am. Chem. Soc.* **2011**, *133*, 9178-9180; c) T. Nakazono, A. R. Parent, K. Sakai, *Chem. Commun.* **2013**, *49*, 6325-6327; d) E. Pizzolato, M. Natali, B. Posocco, A. M. López, I. Bazzan, M. Di Valentin, P. Galloni, V. Conte, M. Bonchio, F. Scandola, *Chem. Commun.* **2013**, *49*, 9941-9943; e) D. J. Wasylenko, C. Ganesamoorthy, J. Borau-Garcia, C. P. Berlinguette, *Chem. Commun.* **2011**, *47*, 4249-4251; f) M. L. Rigsby, S. Mandal, W. Nam, L. C. Spencer, A. Llobet, S. S. Stahl, *Chem. Sci.* **2012**, *3*, 3058-3062; g) Z. Huang, Z. Luo, Y. V. Geletii, J. W. Vickers, Q. Yin, D. Wu, Y. Hou, Y. Ding, J. Song, D. G. Musaev, C. L. Hill, T. Lian, *J. Am. Chem. Soc.* **2011**, *133*, 2068-2071; h) H. Lv, J. Song, Y. V. Geletii, J. W. Vickers, J. M. Sumliner, D. G. Musaev, P. Kögerler, P. F. Zhuk, J. Bacsa, G. Zhu, C. L. Hill, *J. Am. Chem. Soc.* **2014**, *136*, 9268-9271; i) Y. V. Geletii, B. Botar, P. Kögerler, D. A. Hillesheim, D. G. Musaev, C. L. Hill, *Angew. Chem. Int. Ed.* **2008**, *47*, 3896-3899; j) M. Chen, S.-M. Ng, S.-M. Yiu, K.-C. Lau, R. J. Zeng, T.-C. Lau, *Chem. Commun.* **2014**, *50*, 14956-14959.

[18] a) L. Duan, F. Bozoglian, S. Mandal, B. Stewart, T. Privalov, A. Llobet, L. Sun, *Nat. Chem.* **2012**, *4*, 418-423; b) L. Duan, L. Wang, F. Li, F. Li, L. Sun, *Acc. Chem. Res.* **2015**, 48, 2084–2096.

[19] a) L. Tong, M. Gothelid, L. Sun, *Chem. Commun.* **2012**, *48*, 10025-10027; b) Y. Chen, H. Chen, H. Tian, *Chem. Commun.* **2015**, *51*, 11508-11511.

[20] S. Dey, B. Mondal, A. Dey, *Phys. Chem. Chem. Phys.* **2014**, *16*, 12221-12227.

[21] A. Han, H. Wu, Z. Sun, H. Jia, Z. Yan, H. Ma, X. Liu, P. Du, *ACS Appl. Mater. Interfaces* **2014**, *6*, 10929-10934.

[22] K. S. Joya, K. Takanabe, H. J. De Groot, *Adv. Energy Mater.* **2014**, *4, 1400252*.

[23]D. Hong, J. Jung, J. Park, Y. Yamada, T. Suenobu, Y.-M. Lee, W. Nam, S. Fukuzumi, *Energy Environ. Sci.* **2012**, *5*, 7606-7616.

[24] T. Zhang, C. Wang, S. Liu, J.-L. Wang, W. Lin, *J. Am. Chem. Soc.* **2014**, *136*, 273-281.

[25] K. S. Joya, N. K. Subbaiyan, F. D'Souza, H. J. de Groot, *Angew. Chem. Int. Ed.* **2012**, *51*, 9601-9605.

[26] B. S. Yeo, A. T. Bell, *J. Am. Chem. Soc.* **2011**, *133*, 5587-5593.

[27] D. Ressnig, M. Shalom, J. Patscheider, R. Moré, F. Evangelisti, M. Antonietti, G. R. Patzke, *J. Mater. Chem. A* **2015**, *3*, 5072-5082.

[28] A. M. Ullman, Y. Liu, M. Huynh, D. K. Bediako, H. Wang, B. L. Anderson, D. C. Powers, J. J. Breen, H. D. Abruña, D. G. Nocera, *J. Am. Chem. Soc.* **2014**, *136*, 17681-17688.

[29] J J. Goldstein, D. E. Newbury, P. Echlin, D. C. Joy, A. D. Romig Jr, C. E. Lyman, C. Fiori, E. Lifshin, Scanning electron microscopy and X-ray microanalysis: a text for biologists, materials scientists, and geologists, Springer Science & Business Media, **2012**

[30] a) N. S. McIntyre, M. G. Cook, *Anal. Chem.* **1975**, *47*, 2208-2213; b) C. A. Kent, J. J. Concepcion, C. J. Dares, D. A. Torelli, A. J. Rieth, A. S. Miller, P. G. Hoertz, T. J. Meyer, *J. Am. Chem. Soc.* **2013**, *135*, 8432-8435; c) F. Song, Y. Ding, B. Ma, C. Wang, Q. Wang, X. Du, S. Fu, J. Song, *Energy Environ. Sci.* **2013**, *6*, 1170-1184; d) J. Matthew, *Surf. Interface Anal.* **2004**, *36*, 1647-1647.

[31] a) S. D. Techane, L. J. Gamble, D. G. Castner, *T J. Phys. Chem. C* **2011**, *115*, 9432-9441; b) N. Wu, L. Fu, M. Su, M. Aslam, K. C. Wong, V. P. Dravid, *Nano lett.* **2004**, *4*, 383-386.

[32] S. C. Petitto, E. M. Marsh, G. A. Carson, M. A. Langell, *J. Mol. Catal. A: Chem.* **2008**, *281*, 49-58.

[33] S. Ciampi, T. Böcking, K. A. Kilian, M. James, J. B. Harper, J. J. Gooding, *Langmuir* **2007**, *23*, 9320-9329.

[34] R. L. Arechederra, K. Artyushkova, P. Atanassov, S. D. Minteer, *ACS Appl. Mater. Interfaces* **2010**, *2*, 3295-3302.

[35] P. Garrido-Barros, I. Funes-Ardoiz, S. Drouet, J. Benet-Buchholz, F. Maseras, A. Llobet, *J. Am. Chem. Soc.* **2015**, *137*, 6758-6761.

[36] *Lide, David R., ed. CRC handbook of chemistry and physics. Vol. 85. CRC press, **2004**.*

[37] a) J. Rossmeisl, Z. W. Qu, H. Zhu, G. J. Kroes, J. K. Norskov, *J Electroanal. Chem.* **2007**, *607*, 83-89; b) J. Rossmeisl, A. Logadottir, J. K. Norskov, *Chem. Phys.* **2005**, *319*, 178-184.

[38] a) J. O. Bockris, T. Otagawa, *J. Phys. Chem-Us* **1983**, *87*, 2960-2971; b) M. Busch, E. Ahlberg, I. Panas, *Phys. Chem. Chem. Phys.* **2011**, *13*, 15069-15076.

[39] I. C. Man, H. Y. Su, F. Calle-Vallejo, H. A. Hansen, J. I. Martinez, N. G. Inoglu, J. Kitchin, T. F. Jaramillo, J. K. Norskov, J. Rossmeisl, *Chemcatchem* **2011**, *3*, 1159-1165.

[40] R. Frydendal, M. Busch, N. B. Halck, E. A. Paoli, P. Krtil, I. Chorkendorff, J. Rossmeisl, *Chemcatchem* **2015**, *7*, 149-154.

[41] a) N. B. Halck, V. Petrykin, P. Krtil, J. Rossmeisl, *Phys Chem Chem Phys* **2014**, *16*, 13682-13688; b) M. Busch, N. B. Halck, U. I. Kramm, S. Siahrostami, P. Krtil, J. Rossmeisl, *Nano Energy* **2016**, http://dx.doi.org/10.1016/j.nanoen.2016.04.011i

[42] J. M. de Ruiter, R. L. Purchase, A. Monti, C. J. M. van der Ham, M. P. Gullo, K. S. Joya, M. D'Angelantonio, A. Barbieri, D. G. H. Hetterscheid, H J. M. de Groot, F. Buda, *ACS Catal.* **2016**, *6*, 7340-7349.

[43] a) M. D. Wodrich, M. Busch, C. Corminboeuf, *Chem. Sci.* **2016**, *7*, 5723-5735; b) M. Busch, M. D. Wodrich, C. Corminboeuf, *Chem. Sci.* **2015**, *6*, 6754-6761; c) R. Parsons, *T Faraday Soc* **1958**, *54*, 1053-1063; d) J. K. Norskov, T. Bligaard, J. Rossmeisl, C. H. Christensen, *Nat. Chem.* **2009**, *1*, 37-46; e) H. Gerischer, *Bulletin des Sociétés Chimiques Belges* **1958**, *67*, 506-527.

[44] P. Sabatier, *La Catalyse en Chimie Organique, Librarie Polytechnique, Paris* **1993**.

[45] M. Lehtimaki, H. Hoffmannova, O. Boytsova, Z. Bastl, M. Busch, N. B. Halck, J. Rossmeisl, P. Krtil, *Electrochim. Acta* **2016**, *191*, 452-461.

[46] M. Bajdich, M. Garcia-Mota, A. Vojvodic, J. K. Norskov, A. T. Bell, *J. Am. Chem. Soc.* **2013**, *135*, 13521-13530.

[47] O. Diaz-Morales, I. Ledezma-Yanez, M. T. M. Koper, F. Calle-Vallejo, *ACS Catal.* **2015**, *5*, 5380-5387.

[48] S. Chu, E. Coccia, M. Barborini, L. Guidoni, *J. Chem. Theory Comput.* **2016**. DOI: 10.1021/acs.jctc.6b00632.

[49] F. H. Hodel, S. Luber, *ACS Catal.* **2016**, *6*, 1505-1517.

[50] F. Acuna-Pares, Z. Codola, M. Costas, J. M. Luis, J. Lloret-Fillol, *Chem-Eur. J.* **2014**, *20*, 5696-5707.

[51] D. E. Polyansky, J. T. Muckerman, J. Rochford, R. F. Zong, R. P. Thummel, E. Fujita, *J. Am. Chem. Soc.* **2011**, *133*, 14649-14665.

[52] X. J. Su, M. Gao, L. Jiao, R. Z. Liao, P. E. M. Siegbahn, J. P. Cheng, M. T. Zhang, *Angew. Chem. Int. Ed.* **2015**, *54*, 4909-4914.

[53] a) F. Calle-Vallejo, J. I. Martinez, J. M. Garcia-Lastra, E. Abad, M. T. M. Koper, *Surf. Sci.* **2013**, *607*, 47-53; b) M. T. M. Koper, *J Electroanal. Chem.* **2011**, *660*, 254-260.

[54] C. J. Cramer, D. G. Truhlar, *Phys. Chem. Chem. Phys.* **2009**, *11*, 10757-10816.

[55] S. Trasatti, *Electrochim. Acta* **2000**, *45*, 2377-2385.

[56] D. Friebel, M. W. Louie, M. Bajdich, K. E. Sanwald, Y. Cai, A. M. Wise, M. J. Cheng, D. Sokaras, T. C. Weng, R. Alonso-Mori, R. C. Davis, J. R. Bargar, J. K. Norskov, A. Nilsson, A. T. Bell, *J. Am. Chem. Soc.* **2015**, *137*, 1305-1313.

FULL PAPER

An *in-situ* generated cobalt catalyst efficiently conduct photochemical as well as electrochemical water oxidation at near-neutral conditions. The catalyst film, assembled during electrochemcal WO, exhibited low overpotential of 360 mV and high oxygen evolution peak current density of 9 mA cm^{-2} on GC electrode at only 1.49 (*vs*. NHE), under neutral conditions. This work shed light upon the ability of the direct assembling molecular metal-organic catalyst films on the surface of different conducting electrodes giving a chance towards the molecular engineering of a cobalt-based electrocatalytic films.

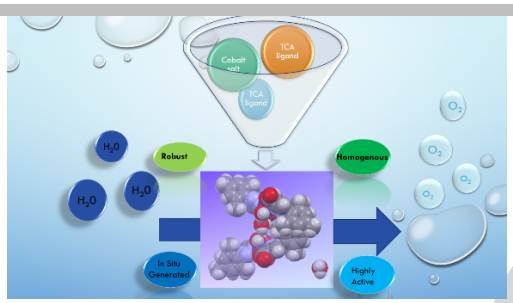

*Hussein. A. Younus, Nazir Ahmad, Adeel H. Chughtai, Matthias Vandichel, Michael Busch, Kristof Van Hecke, Mekhman Yusubov, Shaoxian Song, Francis Verpoort**

Page No. – Page No.
A robust molecular catalyst generated *in-situ* for photo- and electrochemical water oxidation